

**NUMERICAL EVIDENCE OF DYNAMICAL SPECTRAL  
RIGIDITY OF ELLIPSES AMONG SMOOTH  $\mathbb{Z}_2$ -SYMMETRIC  
DOMAINS**

SHANZA AYUB AND JACOPO DE SIMOI

ABSTRACT. We present numerical evidence for spectral rigidity among  $\mathbb{Z}_2$ -symmetric domains of ellipses of eccentricity smaller than 0.30.

1. INTRODUCTION

The famous question “Can one hear the shape of a drum?” posed by M. Kac in [7] has motivated over 50 years of research into what is now called the *Inverse Spectral Problem*. In this paper we present numerical evidence to support a conjecture that is closely related to this problem.

Let us introduce the main concepts so that we can present our results. In this paper a *domain* will refer to a subset  $\Omega \subset \mathbb{R}^2$  which is open, connected, bounded and whose boundary  $\partial\Omega$  is a sufficiently smooth curve; for simplicity<sup>1</sup> we consider here domains with  $C^\infty$  boundary. We denote with  $\mathcal{D}$  the set of all such domains.

Given a domain  $\Omega \in \mathcal{D}$ , we denote its *Laplace Spectrum* with

$$\mathrm{Sp}(\Omega) = \{0 < \lambda_0 \leq \lambda_1 \leq \dots \leq \lambda_k \leq \dots\}$$

where the  $\lambda_i$  are the eigenvalues of the Dirichlet<sup>2</sup> Boundary Problem, i.e. those  $\lambda$  for which there exists  $u \in L^2(\Omega)$  so that:

$$\begin{aligned} \Delta u(x) + \lambda u(x) &= 0 \text{ if } x \in \Omega \\ u(x) &= 0 \text{ if } x \in \partial\Omega. \end{aligned}$$

Kac’s question can be then expressed, more formally, as “Does  $\mathrm{Sp}(\Omega)$  determine  $\Omega$ ?”. Clearly, domains that are isometric to each other (i.e. can be obtained by one another via a composition of rotations and translations) will have the same Laplace spectrum. From now on we will, in this paper, identify isometric domains, i.e. we consider two domains to be equal if they are isometric. Two domains  $\Omega$  and  $\Omega'$  are said to be *Laplace isospectral* if  $\mathrm{Sp}(\Omega) = \mathrm{Sp}(\Omega')$ . We can thus further rephrase Kac’s question as: “Are isospectral domains necessarily isometric?”

In full generality, this question has a negative answer: in [11] the authors construct an explicit example of a pair of isospectral domains that are not isometric,

---

*Date:* June 12, 2020.

<sup>1</sup> Our discussion can be actually applied to domains whose boundary is  $C^8$ -smooth, but we do not want to insist on this point here.

<sup>2</sup> Historically, the majority results in the field have been obtained with Dirichlet boundary conditions, although other type of boundary conditions can be treated and are equally relevant. In this paper we will follow this long established tradition and consider only Dirichlet boundary conditions.

and many more domains can indeed be constructed by similar methods. However all such constructions yield domains that are neither smooth nor convex. In fact Kac's question is still open if we require  $\Omega$  to have a smooth boundary: this problem is indeed notoriously hard. In order to obtain some results with the current technology, some further restrictions on the class of admissible domains are needed.

In order to proceed with our discussion, let us introduce some further notation. Let us fix a class  $\mathcal{M} \subset \mathcal{D}$  of domains; a domain  $\Omega \in \mathcal{M}$  is said to be  *$\mathcal{M}$ -spectrally determined* if there are no other domains in  $\mathcal{M}$  that are isospectral to  $\Omega$ . In other words, let us define the  *$\mathcal{M}$ -isospectral set of  $\Omega$* :

$$\text{Iso}_{\mathcal{M}}(\Omega) = \{\Omega' \in \mathcal{M} \text{ so that } \text{Sp}(\Omega) = \text{Sp}(\Omega')\};$$

then  $\Omega$  is  $\mathcal{M}$ -spectrally determined if  $\text{Iso}_{\mathcal{M}}(\Omega) = \{\Omega\}$ . Moreover, we say that *one can solve the Inverse Spectral Problem in  $\mathcal{M}$*  if every domain  $\Omega \in \mathcal{M}$  is  $\mathcal{M}$ -spectrally determined.

A surprising relation exists between  $\text{Sp}(\Omega)$  and a dynamically determined object, the *Length Spectrum* of  $\Omega$ . Let us recall that, given a domain  $\Omega$ , one can consider the billiard dynamics inside  $\Omega$ ; some trajectories of this dynamics might be *periodic*. Geometrically, periodic billiard trajectories correspond to closed polygons, not necessarily convex, inscribed in  $\Omega$  with the property that, at each vertex, the angles that either of the two sides that join at the vertex form with the tangent line to the boundary are equal to each other (this is the well-known law of optical reflection). The perimeter of such a polygon is said to be the *length* of the corresponding periodic trajectory. The number of sides of such a polygon is called the *period* of the trajectory. The Length Spectrum of  $\Omega$  is then defined as the set:

$$\mathcal{L}(\Omega) = \mathbb{N}\{\text{length of all periodic billiard trajectories of } \Omega\} \cup \mathbb{N}\{|\partial\Omega|\}$$

where  $|\partial\Omega|$  is the length of the boundary of  $\Omega$  and the factor of  $\mathbb{N}$  accounts for the fact that one can always consider a periodic orbit traversed multiple times as a periodic orbit of length equal to a multiple of the original length of the orbit.

The relation between the Laplace Spectrum and the Length Spectrum can be stated as follows: consider the following distribution

$$(1) \quad w(t) := \sum_{\lambda_i \in \text{Sp}(\Omega)} \cos(t\sqrt{\lambda_i})$$

which is called the *wave trace distribution*; then it has been proved in [2] that:

$$(2) \quad \text{sing supp } (w(t)) \subseteq \pm\mathcal{L}(\Omega) \cup \{0\}$$

where  $\text{sing supp } (w(t))$  denotes the *singular support* of  $w(t)$ . Moreover, if  $\Omega$  satisfies some generic conditions, which can be expressed purely in dynamical terms, it has been shown that the inclusion in (2) is indeed an equality: in particular, for generic domains, the Laplace Spectrum determines the Length Spectrum (see e.g. [3, Remark 2.10] and references therein). And so, just how the Inverse Spectral Problem has been posed in terms of the Laplace Spectrum, one can set up an Inverse Problem in terms of the Length Spectrum. A domain  $\Omega \in \mathcal{M}$  is said to be  *$\mathcal{M}$ -dynamically spectrally determined* if  $\Omega$  is the unique element of  $\mathcal{M}$  with the same Length Spectrum. Hence, the Inverse Dynamical Problem asks: is every  $\Omega \in \mathcal{M}$  dynamically spectrally determined?

The inverse problem (either in the Laplace formulation or the dynamical formulation) turns out to be extremely hard (see the next section for some available prior results). A related question, that proved to be more tractable, is the problem of *spectral rigidity*: we say that a domain  $\Omega$  is  $\mathcal{M}$ -spectrally rigid (resp.  $\mathcal{M}$ -dynamically spectrally rigid) if every  $C^1$ -family of domains  $\{\Omega_t\}_{t \in (-\varepsilon, \varepsilon)}$  with  $\Omega_0 = \Omega$  and with the property that  $\text{Sp}(\Omega) = \text{Sp}(\Omega_t)$  (resp.  $\mathcal{L}(\Omega) = \mathcal{L}(\Omega_t)$ ) for any  $t \in (-\varepsilon, \varepsilon)$  is a trivial family (i.e. a family of isometric domains). In other words, a domain  $\Omega$  is  $\mathcal{M}$ -spectrally rigid (resp.  $\mathcal{M}$ -dynamically spectrally rigid) if every  $C^1$ -deformation in  $\mathcal{M}$  preserving the Laplace (resp. Length) Spectrum is necessarily a trivial deformation. Clearly, if a domain is  $\mathcal{M}$ -spectrally determined, then it is  $\mathcal{M}$ -spectrally rigid, but the converse, in general, is not guaranteed to be true.

In this paper we provide some numerical evidence to support the following conjecture:

**Conjecture.** Ellipses are dynamically spectrally rigid among axially-symmetric smooth convex domains.

We will present our results in full detail in Section 4.

**1.1. Related prior results.** It has been shown in [13] that the inverse spectral problem can be solved in a class  $\mathcal{M}$  of domains that are convex, axially-symmetric, analytic and satisfy a generic dynamical condition. However, such results depend crucially on the analyticity assumption, and cannot be extended in any way to the case of smooth domains. Some progress was made in [5], where Hezari and Zelditch showed that if  $\Omega_0$  is an ellipse and  $\Omega_\tau$  is a  $C^1$  Dirichlet (or Neumann) isospectral deformation of  $\Omega_0$  through  $C^\infty$  domains which preserves the  $\mathbb{Z}_2 \times \mathbb{Z}_2$  symmetry group of the ellipse, then it is necessarily *flat* (i.e. all derivatives must vanish for  $\tau = 0$ ). This result shows that ellipses are *infinitesimally spectrally rigid* among  $C^\infty$  domains with the symmetries of the ellipse. Very recently, in [6], the same authors proved that ellipses of small eccentricity are spectrally determined among all  $C^\infty$  domains. This, of course, settles the conjecture that we are investigating for small values of the eccentricity. However, no bound on the *smallness* of eccentricity is provided. We point out that all studies mentioned thus far have used more traditional (i.e. non dynamical) approach to Laplace spectral rigidity and determination (except in [6], where dynamical results obtained in [1] and [8] are crucially employed).

In this paper we rely on the dynamical technique used in [3] to investigate numerically the problem. In [3], the authors prove the *dynamical spectral rigidity* of  $\mathbb{Z}_2$ -symmetric strictly convex domains close to a circle. The proof hinges on the construction, for each  $\mathbb{Z}_2$ -symmetric strictly convex domain  $\Omega$ , of an operator called the *linearized isospectral operator*, which we denote with  $\mathcal{T}_\Omega$ . Then they proved that the injectivity of  $\mathcal{T}_\Omega$  implies the dynamical spectral rigidity of  $\Omega$  among  $\mathbb{Z}_2$ -symmetric strictly convex domains; finally they prove that if  $\Omega$  is sufficiently close to a circle, then the operator  $\mathcal{T}_\Omega$  is injective.

In this paper, we use the method outlined above and compute, numerically, the linearized isospectral operator for ellipses of various eccentricities; we then check numerically whether or not this operator is injective to give evidence for the spectral rigidity of the corresponding ellipse.

**Outline of the paper.** In Section 2, we recall, for the readers' convenience, some definitions regarding elliptic integrals and elliptic functions. In Section 3, we

describe the method discussed in [3] in more detail and explain how it will be used for the purposes of this paper. In Section 4, we present and discuss our numerical results as based on the method described in Section 3. We finally record in the tables in the appendix the values obtained by our numerical investigation.

## 2. ELLIPSES AND ELLIPTIC INTEGRALS

In this section, we recall a few basic definitions and set some important notation used in the rest of the paper. An ellipse centered at the origin with semi-axes oriented along the coordinate axes and of lengths  $0 < b \leq a$  is defined as follows:

$$\mathcal{E}_{a,b} = \left\{ (x, y) \in \mathbb{R}^2 : \frac{x^2}{a^2} + \frac{y^2}{b^2} = 1 \right\}.$$

The value  $a$  is the length of the major semi-axis and  $b$  is the length of the minor semi-axis. We denote the eccentricity of the ellipse with  $e = \sqrt{1 - b^2/a^2} \in [0, 1)$ ; it is a measure of how close the ellipse is to a circle<sup>3</sup>. We let  $c = a \cdot e = \sqrt{a^2 - b^2}$  denote the distance from the center to any of the foci.

We further recall the definitions for Elliptic Integrals and Jacobi Elliptic functions (we also refer the reader to [8] and references therein for a more comprehensive presentation). For  $m \in [0, 1)$ :

- *Incomplete elliptic integral of the first kind*: for  $\varphi \in [0, \pi/2]$  we let

$$F(\varphi | m) := \int_0^\varphi \frac{1}{\sqrt{1 - m \sin^2 \varphi'}} d\varphi';$$

here  $k = \sqrt{m}$  is called the *modulus*; the quantity  $\varphi$  is called the *amplitude*.

- *Complete elliptic integral of the first kind*:

$$K(m) = F(\pi/2 | m).$$

- *Incomplete elliptic integral of the second kind*:

$$E(\varphi | m) = \int_0^\varphi \sqrt{1 - m \sin^2(\varphi')} d\varphi'.$$

- *Complete elliptic integral of the second kind*:

$$E(m) = E(\pi/2 | m).$$

We also recall the *Jacobi elliptic functions*  $\text{sn}(u, m)$  and  $\text{cn}(u, m)$  which are obtained by inverting the incomplete elliptic integrals of the first kind, where  $u$  is called the *argument* and  $m$  is the *modulus* as described earlier. They are defined in such a way that for a given  $m$ , we have  $\text{cn}(u, m) = \cos(\varphi)$  and  $\text{sn}(u, m) = \sin(\varphi)$  where  $\varphi$  is so that  $F(\varphi | m) = u$ ;  $\varphi$  is called the *amplitude* of  $u$  and will be denoted by  $\varphi(u | m)$ .

---

<sup>3</sup>Note that an ellipse with  $e = 0$  is a circle.

## 3. BILLIARD DYNAMICS IN ELLIPSES AND METHODS

In this section we provide definitions relating to the billiard map within an ellipse  $\mathcal{E}$ , we describe the method described in [3] for determining spectral rigidity in our study and we present the details of the implementation of this method.

More precisely, in Section 3.1, we will describe the strategy, proposed in [3], that we will implement for determining spectral rigidity among  $\mathbb{Z}_2$ -symmetric domains; then, in Section 3.2, we will specialize our discussion to the case of ellipses; finally, in Section 3.3, we describe how the numerical computations were carried out in this study.

**3.1. The strategy.** Let  $\Omega$  be a  $\mathbb{Z}_2$ -symmetric domain; to fix ideas we assume that the perimeter  $|\partial\Omega| = 1$ ; since domains are defined up to rigid motions, we can assume the symmetry axis of  $\Omega$  to coincide with the  $x$ -axis. By convexity,  $\partial\Omega$  intersects the symmetry axis in two points: let us choose one of them (arbitrarily) and denote it by  $P$ . Let us further assume (by possibly translating  $\Omega$  along the  $x$ -axis) that the other intersection point of  $\partial\Omega$  with the  $x$ -axis is  $-P$ .

**Proposition 3.1** (see [3, Lemma 4.3]). For any  $q > 2$ , there exist  $q$  points  $(X_0^q, \dots, X_{q-1}^q)$ , with  $X_j^q \in \partial\Omega$ ,  $X_0^q = P$ , which correspond to collision points of a periodic billiard orbit of period  $q$ , with the property that the polygonal curve  $X_0^q X_1^q \dots X_{q-1}^q$  is a simple closed curve.

**Remark 3.2.** If  $q = 2$ , due to symmetry and smoothness of  $\partial\Omega$ , we are guaranteed that  $\partial\Omega$  intersects the  $x$ -axis at a right angle; therefore taking  $X_0^2 = P$  and  $X_1^2 = -P$  yields, in fact, an orbit of the billiard table, which is called the *bouncing ball* orbit. This orbit is, strictly speaking, not *simple*, but will be considered as such in the sequel. The orbits of larger period can always be constructed by variational methods (see e.g. [3, Lemma 4.3]).

In order to be consistent, if several orbits of such type exist, we choose the points  $X_j^q$  so that they give an orbit of maximal length and so that the length of  $X_0^q X_1^q$  is maximal among the orbits of maximal lengths. Moreover, for  $q = 1$ , it turns out to be convenient to define, conventionally,  $X_0^1 = P$ .

Using this sequence of periodic orbits, we proceed to construct the associated so-called *linearized isospectral operator*. In order to do so we need to introduce some more notation. First, by definition of billiard, each collision point  $X_j^q$  is such that the angle between the incoming edge  $X_{j-1}^q X_j^q$  and the tangent vector to  $\partial\Omega$  at  $X_j^q$  equals the angle between the outgoing edge<sup>4</sup>  $X_j^q X_{j+1}^q$  and the same tangent vector. Let us denote this angle by  $\phi_j^q \in (0, \pi)$ . Conventionally, for  $q = 1$ , we define  $\phi_0^1 = \pi/2$ . Next, we introduce a convenient parametrization of  $\partial\Omega$  as follows. Let  $s$  denote the arc-length parametrization of  $\partial\Omega$  with the choice of origin so that  $P$  corresponds to  $s = 0$  and let  $\rho(s)$  denote the *radius of curvature* of  $\partial\Omega$  expressed in terms of  $s$ . Then we define the *Lazutkin parameterization*, denoted by  $x$ , as follows:

$$x(s) = C \int_0^s \rho(s)^{-2/3} ds \quad \text{where } C = \left[ \int_0^1 \rho(s)^{-2/3} ds \right]^{-1}.$$

<sup>4</sup> The subscripts in  $X_j^q$  are considered to be modulo  $q$ .

We also define the *Lazutkin weight* function:

$$\mu(x) = \frac{1}{2C\rho(x)^{1/3}},$$

where  $\rho(x)$  denotes the radius of curvature as a function of the Lazutkin coordinate  $x$ . We refer the reader to [3, Appendix A.2] for an in-depth discussion of properties of this parameterization. We then denote with  $x_j^q$  the Lazutkin coordinate of the collision point  $X_j^q$  (in particular,  $x_0^q = 0$  for any  $q \geq 1$ ).

Then, for any  $q \geq 1$  and  $j \geq 1$  we define the following quantity:

$$(3) \quad \mathcal{T}_{q,j} = \sum_{n=0}^{q-1} \frac{\cos(2\pi j x_n^q)}{\mu(x_n^q)} \sin(\phi_n^q)$$

**Remark 3.3.** The quantities  $\mathcal{T}_{q,j}$  admit the following geometrical interpretation. Consider the deformation of domain  $\Omega$  by the infinitesimal *normal* perturbation described by the function  $n(x)$ ; in other terms, at the point identified by  $x$ , we are deforming  $\partial\Omega$  along the normal direction by  $n(x)$  (outward if  $n(x) > 0$  or inward if  $n(x) < 0$ ). If  $n$  preserves the  $\mathbb{Z}_2$ -symmetry (i.e. it is an even function of  $x$ ), the deformed domain will also be  $\mathbb{Z}_2$ -symmetric; assuming that the orbits found above persist this deformation, they will possibly change their length. For  $q \geq 2$  the quantity  $\mathcal{T}_{q,j}$  corresponds to the variation of the length of the  $q$ -th orbit by the deformation  $n(x) = \cos(2\pi j x)$  (the  $j$ -th Fourier Mode).

The criterion for spectral rigidity of  $\Omega$  that was proposed in [3] can be now loosely stated as follows: if the infinite matrix  $\mathcal{T}_{q,j}$  is not degenerate, then  $\Omega$  is spectrally rigid. In order to properly state the non-degeneracy condition, we find necessary to introduce some other notions.

Remarkably, the following proposition holds (see [3, Lemma B.1 and Lemma 5.3]):

**Proposition 3.4.** For any  $j \geq 1$ , the quantities

$$(4) \quad \varkappa_j = \lim_{q \rightarrow \infty} q^2 \mathcal{T}_{q,j}$$

exist and are finite.

**Remark 3.5.** In the notation of [3], we have the expression

$$\varkappa_j = \tilde{\ell}_\bullet(\cos(2\pi j x)).$$

The values of  $\varkappa_j$  are related to the variation of the first Marvizi–Melrose (see [9]) coefficient of  $\Omega$  by a perturbation that is the  $j$ -th Fourier harmonic in Lazutkin coordinates.

We then define the reduced matrix:

$$\tilde{\mathcal{T}}_{q,j} = \mathcal{T}_{q,j} - \frac{\varkappa_j}{q^2},$$

and, for  $\gamma > 0$ , the sequence spaces:

$$h_\gamma = \{b = (a_i)_{i \geq 0} \in \ell^\infty \text{ s.t. } a_0 = 0 \text{ and } \lim_{j \rightarrow \infty} j^\gamma a_j = 0\}$$

equipped with the norm  $\|b\|_\gamma = \max_{j \geq 0} j^\gamma |a_j|$ . Then (see [3, Lemma 5.3]) the following proposition holds:

**Proposition 3.6.** Let  $\gamma \in (3, 4)$ ; then the matrix  $\tilde{\mathcal{T}}$  acts as an operator  $\tilde{\mathcal{T}} : h_\gamma \rightarrow h_\gamma$ .

Then the following criterion for spectral rigidity holds:

**Theorem 3.7.** *If  $\tilde{\mathcal{T}}$  is injective for some choice of  $\gamma$ , then  $\Omega$  is spectrally rigid among  $\mathbb{Z}_2$ -symmetric domains.*

The above is the criterion that we will use to determine whether or not we can say that an ellipse of given eccentricity is spectrally rigid. We thus need to find an explicitly computable condition for  $\tilde{\mathcal{T}}_{q,j}$  to be injective; we will use the following:

**Proposition 3.8.** Let  $X$  be a Banach space,  $T : X \rightarrow X$  be an operator and  $S : X \rightarrow X$  to be an invertible operator; if  $\|T - S\| < \|S^{-1}\|^{-1}$ , where  $\|\cdot\|$  denotes the operator norm, then  $T$  is invertible; in particular  $T$  is injective.

In our case, choosing  $X = h_\gamma$ ,  $T = \tilde{\mathcal{T}}_{q,j}$  and  $S = \text{Id}$ , we can express the operator norm as:

$$\begin{aligned} \|\tilde{\mathcal{T}} - \text{Id}\| &= \max_q \left( q^\gamma \sum_{j=0}^{\infty} j^{-\gamma} |\tilde{\mathcal{T}}_{q,j} - \text{Id}_{q,j}| \right) \\ (5) \quad &= \max_q \left( q^\gamma \sum_{j=1}^{\infty} j^{-\gamma} \left| \mathcal{T}_{q,j} - \delta_{qj} - \frac{\varkappa_j}{q^2} \right| \right) \quad \text{where} \quad \delta_{qj} = \begin{cases} 1 & j = q \\ 0 & \text{otherwise} \end{cases} \end{aligned}$$

In the next section we specialize the above discussion to the setting of elliptical domains.

**3.2. Dynamics in an elliptical billiard table.** To fix ideas, we fix the family of ellipses in such a way that, for each ellipse in the family, its center lies at the origin, its major axis lies along the x-axis (observe that the major axis is a symmetry axis for  $\mathcal{E}$ ) and its circumference (or perimeter), denoted by  $|\mathcal{E}|$ , equals 1. We choose  $P$  to be the point  $(a, 0) \in \mathcal{E}$ , that is the intersection of  $\mathcal{E}$  with the positive  $x$  semi-axis.

**Remark 3.9.** Since ellipses have a  $\mathbb{Z}_2 \times \mathbb{Z}_2$  symmetry, we could also consider the minor axis as an axis of symmetry. This choice seems not to affect our results. See Item i in Section 4.

Given an ellipse, we consider its parametrization by the *amplitude*  $\varphi$  as

$$X(\varphi) = (a \sin(\varphi), -b \cos(\varphi)).$$

Observe that with this choice of  $\varphi$ , the point  $X(0)$  corresponds to the lowest point  $(0, -b)$  of the ellipse. In particular<sup>5</sup> we have  $P = X(\pi/4)$ .

The *arc-length parametrization*, denoted by  $s$ , can then be obtained observing that  $\frac{ds}{d\varphi} = \sqrt{a^2 \cos^2(\varphi) + b^2 \sin^2(\varphi)} = a\sqrt{1 - e^2 \sin^2(\varphi)}$ ; since  $P$  corresponds to  $s = 0$ , we conclude:

$$s(\varphi) = a(E(\varphi|e^2) - E(e^2));$$

in particular we have:

$$|\mathcal{E}| = 4aE(e^2).$$

---

<sup>5</sup> This non-standard choice of origin for the parametrization  $\varphi$  simplifies some formulae in Lazutkin coordinates.

In particular, if we fix  $e \in [0, 1)$  and  $|\mathcal{E}| = 1$ , the value of  $a$  is determined from the above expression;  $b$ , could then be found using the definition of  $e$ . Our family of ellipses will then be parameterized by their eccentricity.

The first ingredient in the analysis recalled in Section 3.1 is the determination of a sequence of periodic orbit of increasing period. This is particularly convenient to do inside an ellipse; we follow the approach in [8] and we refer to their work for further details. Here we limit ourselves to state their observations without proofs.

In our discussion, we assume  $e$  (and therefore  $\mathcal{E}$ ) to be fixed once and for all.

Let us start by considering the family of ellipses confocal to  $\mathcal{E}$  and contained within  $\mathcal{E}$ ; such family of ellipses can be parameterized by  $0 < \lambda < b$  as follows:

$$\mathcal{C}_\lambda = \left\{ (x, y) \in \mathbb{R}^2 : \frac{x^2}{a^2 - \lambda^2} + \frac{y^2}{b^2 - \lambda^2} = 1 \right\}.$$

Notice that for  $\lambda \rightarrow 0$ ,  $\mathcal{C}_\lambda$  approaches  $\mathcal{E}$  and for  $\lambda \rightarrow b$ ,  $\mathcal{C}_\lambda$  approaches the segment joining the two foci.

Let us fix an orientation for  $\mathcal{C}_\lambda$ ; to fix ideas we will always take the counterclockwise orientation. For any  $\lambda \in (0, b)$ , let us proceed with the following inductive geometrical construction: let  $P_0 = P$ ; then given  $P_n \in \mathcal{E}$ , since  $\mathcal{C}_\lambda$  is convex, there exists a unique point  $P_{n+1} \in \mathcal{E}$ , so that the segment  $P_n P_{n+1}$  is tangent to  $\mathcal{C}_\lambda$  and is co-oriented with  $\mathcal{C}_\lambda$ . It turns out<sup>6</sup> that the points  $\{P_n\}$  form a sequence of collision points of a billiard orbit. The ellipse  $\mathcal{C}_\lambda$  is a *caustic* for this billiard orbit. Now, given  $n > 0$ , we can define  $p_n$  the *winding number of  $P_n$*  as the number of times that the polygonal path  $P_0 P_1 P_2 \cdots P_n P_0$  winds around the origin<sup>7</sup>. For any given orbit it can be proved (see for instance [12]) that the ratio  $p_n/n$  converges to some number  $\omega \in (0, 1/2)$  that we call the *rotation number of the orbit*. For some particular values of  $\lambda$ , the corresponding orbit is *periodic*; in particular the rotation number is rational and it is given by the ratio of the winding number of the orbit  $p_q$  and its period  $q$ . For the purposes of our study, we will only consider periodic orbits with rotation number  $1/q$ . Such orbits are so that their trajectory is a simple closed curve (recall Proposition 3.1).

Following [8], let us define  $m_\lambda = \frac{a^2 - b^2}{a^2 - \lambda^2}$ ; notice that by definition we have  $m_\lambda \in (e^2, 1)$ . Then the rotation number  $\omega_\lambda$  of the orbit associated to the caustic  $\mathcal{C}_\lambda$  is (see [8]):

$$(6) \quad \omega_\lambda = \frac{\delta_\lambda}{4K(m_\lambda)} \quad \text{where} \quad \delta_\lambda = 2F(\sin^{-1}(\lambda/b), m_\lambda).$$

Correspondingly, the collision points  $P_n = (x_n, y_n)$  can be obtained by the formula:

$$(7) \quad X_n = (a \cdot \text{sn}(u_n, m_\lambda), -b \cdot \text{cn}(u_n, m_\lambda)) \quad \text{where} \quad u_n = K(m_\lambda) + n\delta_\lambda.$$

The above formula yields the collision points corresponding to the given choice of  $\lambda$ . In order to find the periodic orbits described by Proposition 3.1, it thus suffices, for any  $q$ , to find  $\lambda_q$  so that  $\omega_{\lambda_q} = 1/q$ . Correspondingly  $\delta_{\lambda_q} = 4K(m_{\lambda_q})/q$  and in particular we obtain

$$u_n^q = 4K(m_{\lambda_q}) \left( \frac{n}{q} + \frac{1}{4} \right).$$

<sup>6</sup> This fact is peculiar for elliptical billiards and follows from Poncelet's Porism

<sup>7</sup> A more precise definition of the winding number can be given, but we avoid giving it here, since this definition will suffice for our uses below.



Observe that the periodic orbit of period 2, corresponding to rotation number  $1/2$  cannot be obtained by this process, as it corresponds to the limiting case  $\lambda \rightarrow b$ ; however, it corresponds to the orbit bouncing along the major axis (see Remark 3.2). As in the previous section, we let  $X_j^q$  denote the points in the orbit of period  $1/q$ ; from the expression (7) it is simple to obtain (numerically)  $\phi_n^q$ . We now need to find the value of the Lazutkin parametrization  $x_j^q$  at the collision points. Such coordinates could also be easily found numerically, but in the case of ellipses, the Lazutkin parametrization can be analytically expressed in terms of Elliptic Integrals: in fact, recall the expression for the radius of curvature of an ellipse:

$$\rho(\varphi) = \frac{a}{\sqrt{1-e^2}}(1-e^2 \sin^2(\varphi))^{3/2}.$$

Then substituting the above formula in the expression for the Lazutkin coordinate  $x$ , we conclude:

$$x(\varphi) = \frac{F(\varphi | e^2) - K(e^2)}{4K(e^2)} \quad \text{and} \quad C = \left[4K(e^2)a^{1/3}(1-e^2)^{1/3}\right]^{-1}.$$

and

$$\mu(\varphi) = 2K(e^2)\sqrt{\frac{1-e^2}{1-e^2 \sin^2 \varphi}}.$$

In particular, for the periodic orbit of period  $q$  we conclude:

$$(8) \quad x_n^q = \frac{F(\varphi(u_n^q | m_{\lambda_q}) | e^2) - K(e^2)}{4K(e^2)}$$

Observe that, as  $q \rightarrow \infty$ ,  $m_{\lambda_q} \rightarrow e^2$  and  $x_n^q \rightarrow n/q$ .

**3.3. Details of our numerical implementation.** Here we list the tasks that we implemented numerically. The code has been written in *Python* and can be found in this GitHub repository.

First of all, we considered orbits of period up to `maxq` and found that setting `maxq=500` was sufficient for our purposes.

- The first task that needs to be implemented is to find the sequence of values  $\lambda_q$  corresponding to periodic orbits of rotation number  $1/q$ ; we performed this computation by numerically inverting the formula (6) for  $\omega_\lambda$  using the bisection method; this computation is implemented in the *Python* method `find_lambda`.
- Once the  $\lambda_q$ 's are found, we proceed to apply (7) and find the collision points  $X_n^q$ ; such points are stored as amplitudes  $\varphi_q^k$  and are calculated in the *Python* method `find_collision_pts`.
- We need then, given the value  $e$  of eccentricity, to compute the values  $\mathcal{T}_{q,j}$  for sufficiently many  $q$ 's and  $j$ 's according to (3). To this end we need to obtain the angles  $\phi_q^n$ ; such computations are carried out by the *Python* method `sinphi_lst`. The method `T_of_q_j` computes the values of the matrix  $\mathcal{T}_{q,j}$ .

Once these methods are in place, we proceed with the actual computation of the norms. Here we report in detail our strategy:

- We fix an eccentricity  $e \in (0, 1)$ ;  $e$  will sample various intervals in  $(0, 1)$ , depending on the chosen value of  $\gamma$ .

- Since the values  $\varkappa_j$  (defined in (4)) do not depend on  $q$ , we cache them in the list `lambda_MM`; observe that, due to the extra symmetries of the ellipse,  $\varkappa_j = 0$  if  $j$  is odd. In order to approximate the evaluation of the limit (4), we compute a term with sufficiently large  $q$ , until the difference of the values for  $q$  and  $q + 1$  falls below a certain threshold (we took  $10^{-6}$ ).
- In order to compute numerically (5), we need to truncate the series to some value  $J$ , and stop at some  $Q$  when computing the max. Below we explain how the two cutoffs  $J$  and  $Q$  have been chosen in our investigation:
  - due to the factor  $q^\gamma j^{-\gamma}$ , the larger  $q$  is, the higher the number of  $j$ 's that contribute substantially to the sum. We decided to cut off the series at  $J = C \cdot q$ . Observe that dropping the tail after this cutoff leads to an error of order  $C^{-\gamma+1}$ . In our computations we took  $C = 100$ .
  - the choice of the cutoff  $Q$  depends on the eccentricity by means of the following argument: as  $q$  increases, the values of  $\mathcal{T}_{q,j}$  should approach to the corresponding values for the case of a circle. It is not difficult to compute such values explicitly: for the circle  $\varkappa_j = 0$  for any  $j$  and  $\mathcal{T}_{q,j}$  can be computed explicitly (see [3]); let us denote the operator for the circle as  $\mathcal{T}_{q,j}^0$ ; we then obtain that

$$\begin{aligned} q^\gamma \sum_{j=1}^{\infty} j^{-\gamma} | \mathcal{T}_{q,j}^0 - \delta_{qj} | &= |c_q - 1| + c_q \sum_{s=2}^{\infty} s^{-\gamma} = \\ &= 1 + c_q(\zeta(\gamma) - 2), \end{aligned}$$

where  $\zeta$  is the Riemann Zeta function and

$$c_q = \begin{cases} \pi^{-1} & \text{if } q = 1 \\ \frac{\sin(\pi/q)}{\pi/q} & \text{otherwise.} \end{cases}$$

We then stop our computations as soon as the value of the  $q$ -th entry is within a reasonable accord with the value for the circle. We fix this accord to be 10%.

- the choice of the parameter  $\gamma$  has been made to find a compromise with the computational time. In fact, as  $\gamma \rightarrow 3$ , the quantity  $\|\tilde{\mathcal{T}}_{q,j} - \text{Id}\|_\gamma$  tends to decrease, but computational times tend to increase. Hence, we fixed  $\gamma = 3.5$  for a broad range of eccentricities and then computed the norms with  $\gamma = 3.1$  and  $\gamma = 3.01$  in narrower ranges.

#### 4. RESULTS AND CONCLUDING REMARKS

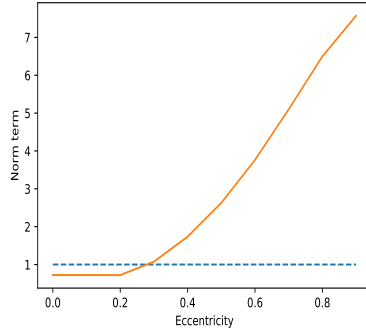
We can now present the numerical evidence we collected by the methods described in Sections 3. This data suggests that the following result should hold.

**Conjecture.** Ellipses of eccentricity  $e \in (0, 0.3)$  are dynamically spectrally rigid among  $\mathbb{Z}_2$ -symmetric smooth convex domains.

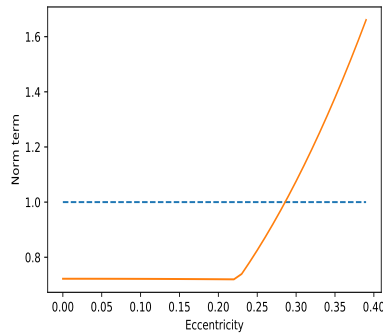
The value 0.3 is certainly an artifact of our method and does not represent a natural threshold.

While we found collision points for eccentricities,  $0 < e < 1$  with step size 0.01, in the interest of computational time it took for the script to run, we divided our analysis into stages. First, we found the norm terms for  $0 < e < 1$  with a step-size

of 0.1 (see Figure 1a), and successively refined the step-size in more narrow ranges.



(A) Values of the norm terms for  $\gamma = 3.5$  and eccentricities,  $e \in [0, 1)$ , with a step size of 0.1.



(B) Values of the norm terms for  $\gamma = 3.5$  and eccentricities,  $e \in [0, 0.4)$ , with a step size of 0.01.

FIGURE 1. Plots for Norm terms vs eccentricities for the two cases the script was run. (a) The eccentricities,  $e \in [0, 1)$ , with a step size of 0.1. The norm terms stay well below 1 until  $e = 0.2$ , but after 0.2 they start to increase and surpass 1 at  $e = 0.3$ , and continue to grow. (b) The eccentricities,  $e \in [0, 0.4)$ , with a step size of 0.01. The norm terms stay well below 1 until  $e = 0.2$ , but after 0.2 they start to increase and surpass 1 at  $e = 0.28$ , and continue to grow past  $e = 0.3$ .

For the choice  $\gamma = 3.5$ , we observed that the norm terms ranged from 0.722 to 7.573, as  $e$  ranged from 0 to 0.9. The terms stayed close to an approximate value of 0.72 for  $e = 0, 0.1$  and 0.2, but then increase to 1.08 for  $e = 0.3$  and 1.74 for  $e = 0.4$ . (For the norm terms generated for each eccentricity in this case, we refer the reader to table 1, Appendix A, Supplementary Materials). In all cases

for  $e > 0.22$ , the largest norm term was reached when  $q = 3$  (for cases  $e \leq 0.22$ , the largest norm term was reached when  $q = 1$ ), after which they decayed (but appeared to increase again after  $q = 20$ ). We cannot exclude that this is caused by numerical instability<sup>8</sup> and so we stopped the computation once the terms were under 0.5. In the case where the terms never went below 1, such as the case was for  $e = 0.9$ , the computation was stopped at  $q = 30$ .

Figure 1a shows that after  $e = 0.4$ , the terms are well past 1, and so we took a closer look at eccentricities below 0.4. Hence, we carried out the computations for  $0 < e < 0.4$  with a step-size of 0.01 to better locate the  $e$  at which the terms crosses the value 1 (see Figure 1b).

We found that in this case, the terms stayed relatively close to a value of 0.72 (obtained for  $q = 1$ ) until  $e = 0.22$ , indicated by the almost horizontal line in Figure 1b, after which they increased to 0.82 for  $e = 0.25$ , surpassing 1 at  $e = 0.29$ . (For the norm terms generated for each eccentricity in this case, we refer the reader to table 2, Appendix A, Supplementary Materials). The norm terms were observed to be equal to 0.97 at  $e = 0.28$  and equal to 1.022 at  $e = 0.29$ , indicating that the matrix  $\mathcal{T}_{q,j}$  might no longer be invertible once  $e > 0.28$ . We then modified the value of  $\gamma$  and explored a narrower range of eccentricities. A choice of  $\gamma = 3.1$  gave a maximum norm term of approximately 0.85 for this eccentricity. It also gave a norm term of 0.968 for  $e = 0.32$ . We investigated what would happen if we were to choose  $\gamma = 3.01$ , but this only extended the range of eccentricities to  $e \leq 0.33$  as it gave a norm term of approximately 0.98 (see Figure 2). All of these computations took a total of approximately 8 hours to run<sup>9</sup>. Higher eccentricities were not included in the computations involving smaller values for  $\gamma$ , as computational time becomes an issue.

An interesting result we noticed was that the maximum norm term was consistently achieved for  $q = 3$  for  $e > 0.22$ , and it was also observed that after  $e \geq 0.15$ , the terms tended to decrease for  $q = 2$  but then increase for  $q = 3$  before steadily decreasing again.

**4.1. Remarks and Future Suggestions.** In this section we make some remarks on our results described in the previous section, as well as some recommendations that could improve the results of this report.

- (i) The ellipse has two axis of symmetry. We performed a similar analysis considering perturbations preserving the symmetry along the minor axis and found no difference in the outcome: ellipses appears to be spectrally rigid at least up to  $e = 0.3$
- (ii) We note here that our choice of  $\gamma$  was rather arbitrary. The method described in [3] only requires  $\gamma$  to be such that  $\gamma \in (3, 4)$  for which  $\|\tilde{\mathcal{T}}_{q,j} - \text{Id}\| < 1$ . As shown in [3], the norm terms decay with a rate of  $Cq\gamma^{-3}$ , hence the smaller the value for  $\gamma$  used, the slower the decay, and correspondingly, the longer the computational time. For the norm terms generated for each eccentricity in these cases, we refer the reader to tables 3 and 4, Appendix A, Supplementary Materials.

<sup>8</sup>This may be due to the system's sensitivity to initial conditions. If the conditions were highly accurate, we would see the terms to decay continuously.

<sup>9</sup>The computation with  $\gamma = 3.1$  was run for  $e \in [0.25, 0.4]$ , and with  $\gamma = 3.01$  was run for  $e \in [0.32, 0.4]$ .

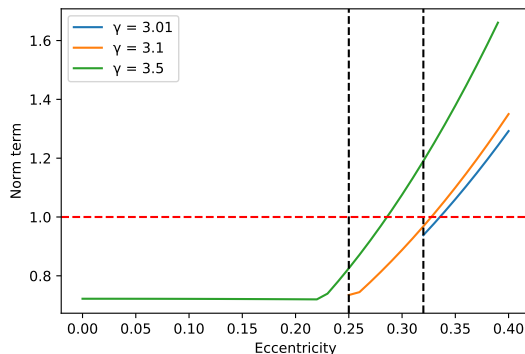


FIGURE 2. Norm terms vs eccentricity with different values of  $\gamma$ : 3.5 (green), 3.1 (orange), 3.01 (blue). The dotted lines denote the eccentricity at which each was run,  $\gamma = 3.1$  was run for  $0.25 < e < 0.4$  and  $\gamma = 3.01$  was run for  $0.32 < e < 0.4$ . The norm terms exceeded 1 for  $e > 0.32$  with  $\gamma = 3.1$  and for  $e > 0.33$  with  $\gamma = 3.01$ .

- (iii) So far in our work we have chosen  $S = \text{Id}$  to determine whether or not the operator was invertible, by means of Proposition 3.8. However, one could choose different operators  $S$ ; a natural choice would be  $S = \mathcal{T}^0$  (recall that  $\mathcal{T}^0$  is the operator  $\mathcal{T}$  for the circle). This should improve the range of eccentricities for which we are able to provide numerical evidence of spectral rigidity, but most likely the improvement would not be substantial.

More interestingly, the finding that the highest norm term was consistently achieved for  $q = 3$  could be further exploited to construct an operator  $S$  which could be more efficient in comparing with  $\mathcal{T}$ . In our work, after the norm terms for  $q > 3$  seemed to decay quickly and the term  $q = 3$  would often be the only term above 1. Constructing a suitable operator would possibly lead to substantial improvements in the range of confidence of our numerical explorations.

## 5. APPENDIX A: SUPPLEMENTARY MATERIALS

TABLE 1. Table showing the Norm terms generated for  $e \in [0, 1)$  with a step size of 0.1.

Eccentricity	Norm Term
0.00	0.7220
0.10	0.7215
0.20	0.7202
0.30	1.0757
0.40	1.7370
0.50	2.6304
0.60	3.7642
0.70	5.1015
0.80	6.4986
0.90	7.5732

TABLE 2. Table showing the norm terms generated for  $e \in [0, 0.4)$  with a step size of 0.01.

Eccentricity	Norm Term
0.00	0.7220
0.01	0.7220
0.02	0.7220
0.03	0.7219
0.04	0.7219
0.05	0.7219
0.06	0.7218
0.07	0.7218
0.08	0.7217
0.09	0.7216
0.10	0.7215
0.11	0.7214
0.12	0.7213
0.13	0.7212
0.14	0.7211
0.15	0.7210
0.16	0.7208
0.17	0.7207
0.18	0.7205
0.19	0.7204
0.20	0.7202
0.21	0.7200
0.22	0.7198
0.23	0.7393
0.24	0.7814

0.25	0.8254
0.26	0.8714
0.27	0.9194
0.28	0.9695
0.29	1.0216
0.30	1.0757
0.31	1.1320
0.32	1.1904
0.33	1.2510
0.34	1.3137
0.35	1.3786
0.36	1.4458
0.37	1.5151
0.38	1.5868
0.39	1.6607

TABLE 3. Table showing the Norm terms generated for  $e \in [0.25, 0.4]$  with  $\gamma = 3.1$ .

Eccentricity	Norm Term
0.25	0.7345
0.26	0.7444
0.27	0.7782
0.28	0.8133
0.29	0.8499
0.30	0.8879
0.31	0.9274
0.32	0.9683
0.33	1.0107
0.34	1.0546
0.35	1.1000
0.36	1.1469
0.37	1.1954
0.38	1.2453
0.39	1.2969
0.40	1.3500

TABLE 4. Table showing the Norm terms generated for  $e \in [0.3, 0.4]$  with  $\gamma = 3.01$ .

Eccentricity	Norm Term
0.32	0.9382
0.33	0.9775
0.34	1.0183
0.35	1.0604
0.36	1.1039
0.37	1.1488
0.38	1.1951
0.39	1.2429
0.40	1.2921

Link to the code: [GitHub repository](#)



## REFERENCES

- [1] A. Avila, J. De Simoi and V. Kaloshin. An integrable deformation of an ellipse of small eccentricity is an ellipse. *Ann. of Math. (2)*, **184**: 527–558, 2016.
- [2] K. G. Andersson and R. B. Melrose. The propagation of singularities along gliding rays. *Invent. Math.*, **41**(3):197–232, 1977.
- [3] J. De Simoi, V. Kaloshin and Q. Wei (Appendix B coauthored with H. Hezari), Dynamical Spectral Rigidity among  $\mathbb{Z}_2$ -symmetric strictly convex domains close to a circle, *Ann. of Math.* **186**: 277-314, 2017.
- [4] V. Guillemin and R. Melrose, An Inverse Spectral Result for Elliptical Regions in  $\mathbb{R}^2$ , *Advances in Math.* **32**: 128-148, 1979.
- [5] H. Hezari and S. Zelditch,  $C^\infty$  Spectral Rigidity of the Ellipse, *Anal. PDE* **5**, No. 5, 2012.
- [6] H. Hezari and S. Zelditch, One can hear the shape of ellipses of small eccentricity, *preprint*
- [7] M. Kac. Can one hear the shape of a drum? *Amer. Math. Monthly*, **73**(4, part II):1–23, 1966.
- [8] V. Kaloshin and A. Sorrentino, On the Local Birkhoff Conjecture for Convex Billiards, 2018, arXiv 1612.0919.
- [9] S. Marvizi and R. Melrose, Spectral Invariants of Convex Planar Regions, *J. Differential Geom.* **17**: 475-502, 1982.
- [10] G. Popov and P. Topalov, From KAM Tori to Isospectral Invariants and Spectral Rigidity of Billiard Tables, 2019, arXiv 1602.0315.
- [11] C. Gordon, D. L. Webb, and S. Wolpert, One cannot hear the shape of a drum. *Bull. Amer. Math. Soc. (N.S.)*, **27**(1):134–138, 1992.
- [12] S. Tabachnikov. Geometry and Billiards. *Mathematics Subjects Classification*, 1991.
- [13] S. Zelditch. Inverse spectral problem for analytic domains. II.  $\mathbb{Z}_2$ -symmetric domains. *Ann. of Math.* **170**(1):205–269, 2009.